Step-Current-Approximation Modulation of Multilevel-CSC With Near-Power-Frequency Switching for High-Current Variable-Voltage Application

Ruihang Bai, *Graduate Student Member, IEEE*, Biao Zhao, *Senior Member, IEEE*, Tianji Zhou, Jikang Wang, Yiqing Ma, *Graduate Student Member, IEEE*, Guangke Lin, Yi Wang, Zhanqing Yu, *Member, IEEE*, and Rong Zeng, *Senior Member, IEEE*

***Abstract*—High-current variable-voltage rectifiers with continuously adjustable output are widely applied in industrial manufacturing, such as electrolysis, electrowinning, and dc arc furnaces. Multilevel current-source converter (MCSC) is a potentially feasible solution in these scenarios. In this article, a step-current-approximation modulation (SCAM) for MCSC is proposed. First, the topological constraint of the current-source converter is analyzed to obtain the feasible stepping-current approximation method, which is further optimized based on the gradient of reference current. Moreover, the current balancing algorithm is designed to achieve the dc current balance between modules with the least additional switching behavior. The proposed SCAM and traditional SPWM are compared by simulation, which indicates that SCAM reduces the switching frequency to less than 1/3 of SPWM and realizes the near-power-frequency switching. Finally, the feasibility of SCAM is verified in the hardware-in-the-loop experiment platform. The proposed SCAM is expected to bring the reverse-blocking devices with low ON-state voltage into the application of MCSC. Therefore, the conversion efficiency will be greatly improved, meeting the energy conversion requirements of large-scale industrial manufacturing.**

***Index Terms*—AC–DC converter, current balancing algorithm (CBA), multilevel current-source converter (MCSC), step-current-approximation modulation (SCAM).**

Manuscript received 30 November 2022; revised 24 March 2023 and 9 May 2023; accepted 16 June 2023. Date of publication 20 June 2023; date of current version 28 July 2023. This work was supported by the National Key R&D Program of China under Grant 2022YFB4200800. Recommended for publication by Associate Editor J. Espinoza. *(Corresponding authors: Biao Zhao; Rong Zeng.)*

Ruihang Bai, Biao Zhao, Tianji Zhou, Yiqing Ma, Zhanqing Yu, and Rong Zeng are with the Department of Electrical Engineering, Tsinghua University, Beijing 100084, China (e-mail: brh20@mails.tsinghua.edu.cn; zhao-biao@tsinghua.edu.cn; zhoutj22@mails.tsinghua.edu.cn; myq21@mails.tsinghua.edu.cn; yzq@tsinghua.edu.cn; zengrong@tsinghua.edu.cn).

Jikang Wang and Yi Wang are with the Beijing Sifang Automation Co., Ltd., Beijing 100085, China (e-mail: wangjikang@sf-auto.com; wangyi01@sf-auto.com).

Guangke Lin is with the Huairou Laboratory, Beijing 101400, China (e-mail: linguangke@hrl.ac.cn).

Color versions of one or more figures in this article are available at https://doi.org/10.1109/TPEL.2023.3287922.

Digital Object Identifier 10.1109/TPEL.2023.3287922

I. Introduction

HIGH-current variable-voltage rectifiers with continuously adjustable output are widely applied in industrial fields, such as electrolysis, electrowinning, and dc arc furnaces [1], [2], [3]. In the recent years, as the concept of power-to-gas develops, such devices also have a growing demand in hydrogen–electrolyzer power supply [4], [5], [6], [7]. In these applications, the current reaches to several kiloamps and the voltage is hundreds of volts [8], [9], [10], [11]. When connected to the grid, the rectifiers are required to be grid-friendly, which means high power factor and limited harmonic [8], [9]. Low output ripple is also helpful for efficiency and product quality in electrolysis application [12], [13]. In addition, the converter is required to be cheap and efficient to improve the economy of energy conversion.

At present, the topologies of such converters mainly include silicon-controlled rectifier (SCR) and voltage-source PWM rectifier (VSR). SCR has large capacity, low cost but serious harmonics and low power factor, for which additional filters, phase-shifting transformers, and var compensator are required [14], [15], [16]. In VSR, high-frequency modulation is applied to reduce harmonics and improve power [17], [18]. Besides, VSR is a dc-side boost converter, so additional dc/dc conversion is necessary to meet the applying requirements [19]. High switching frequency and additional conversion lead to higher power loss and cost. A combination of SCR and VSR is proposed in [20] and [21]. The VSR part not only transmits part of power, but also absorbs the harmonic and compensates reactive power caused by SCR. It overcomes the disadvantages of the previous two topologies to some extent, but has not solved the problem of loss caused by high-frequency PWM. Besides, the scheme brings a complex control strategy in the coordination of the two parts. At present, it has not been applied in industry.

Compared with these schemes, the multilevel current-source converter (MCSC) might have potential prospect in ac/dc conversion for high-current variable-voltage application due to its high current output capacity, dc-side buck characteristic, and brilliant ac-side power factor and harmonic performance. There have been numerous researches on MCSC, in which modulation

strategies are SPWM, SVPWM, and their derived methods [22], [23], [24], [25], [26], [27], [28], [29], [30], [31]. The switching frequency reaches up to kilohertz class [25], [31].

However, MCSC has still not been universally applied in industry. An inherent shortcoming is high power loss. In each MCSC module, one of the three bridge arms on both sides keeps flowing through the dc current, which leads to high conducting loss on power electronic devices. This problem is further exacerbated by additional diodes connected in series to asymmetric devices to withstand reverse voltage. Therefore, devices with low ON-state voltage and reverse blocking capability should be considered in MCSC, such as reverse-blocking IGCT devices [32]. In these devices, the switching energy becomes high, for which the modulation for MCSC with low switching frequency is necessary. Otherwise, the switching loss will counteract the optimized efficiency. Recent researches on MCSC mainly focus on ameliorating PWM method [33] and enlarging the capacity [34], but do not radically solve the problem of high switching frequency.

Nearest level modulation (NLM) has been widely used in voltage-source modular multilevel converter (MMC). With a large quantity of modules, it can achieve good harmonic characteristics at low switching frequency [35], [36]. The several-kiloamps output of MCSC leads to large quantity of paralleled modules, for which it is possible to use the level number in place of the modulation frequency to obtain good ac harmonic characteristics. Bintz et al. [20] pointed out that such method may have potential benefits in MCSC, but there is still a lack of research.

The current balancing algorithm (CBA) between modules is usually attached to the modulation. Chandorkar et al. [26] first proposed the principle of current balancing between two modules. The mainstream researches based on PWM propose the method of allocating different switching mode or sectors to each module according to the inductor current and ac voltage [25], [26], [27], or adjusting the reference current waveform of different modules [29]. Bhesaniya and Shukla [30] and Alskran and Simões [31] proposed a unified CBA to switch modules according to inductance current sequencing, but still based on the PWM modulation of high switching frequency. At present, there is no research on CBA for low-frequency modulation.

Considering the situation above, this article proposes the stepping-current-approximation modulation (SCAM) for MCSC with near-power-frequency switching. The rest of the article is organized as follows. Section II deduces the SCAM scheme for MCSC based on its topology constraints. Section III proposes the pulse allocation strategy with only a few extra switching behaviors to realize the dynamic current balancing among the modules. In Section IV, characteristics of SCAM and traditional SPWM are compared in detail. In Section V, the feasibility and performance of SCAM are verified on hardware-in-the-loop experimental platform with a 10-MW hydrogen–electrolyzer load. In Section VI, both the power loss of SCAM-based MCSC and the mechanism of the modified SCAM to improve harmonic are analyzed and discussed. Finally, Section VII concludes this article.

II. Step-Current-Approximation Modulation for MCSC

A. Principle of Step-Current Approximation

In SCAM, alternating reference current is fit by multilevel step waveform, which is alike NLM. For each phase, the ratio of reference current (i_{ac}) to rated dc current of submodules (I_{SM}) is rounded. If the result is positive, the upper arms of this phase is turned ON in the corresponding number of modules. Otherwise, for a negative result, the lower arms are turned ON. Since the monotonicity of the reference current in sinusoidal form changes only twice in one cycle, this modulation method can theoretically achieve a switching frequency equal to that of the fundamental wave.

Each bridge arm in MMC is made up of separate submodules in series, for which the control of different bridge arms is decoupled [see Fig. 1(a)]. Hence NLM of MMC is not constrained by the topology and can independently generate voltage in different phases, as in Fig. 1(c). In contrast, each bridge arm of MCSC is equivalent to the corresponding arms of sub-CSCs in parallel [see Fig. 1(b)]. The topology of CSC constrains that one and only one arm is at conducting state among the three arms at upper and lower side, respectively. Therefore, the envelope of the respective summation of positive and negative current levels is symmetric [see Fig. 1(d)]. The constraint must be considered when the SCAM applied to MCSC modulates ac current waveforms.

B. SCAM Meeting Current-Source-Topology Constraint

Taking the switch function S_X in representation of the switch state of the device T_X in the bridge arms:

$$S_X = \begin{cases} 1, & \text{when } T_X \text{ is on} \\ 0, & \text{when } T_X \text{ is off} \end{cases} \tag{1}$$

and the topology constraint of CSC (one and only one arm is at conducting state among the three arms at upper and lower side, respectively) can be expressed as

$$\begin{bmatrix} S_{\mathrm{pa}i}, S_{\mathrm{pb}i}, S_{\mathrm{pc}i} \\ S_{\mathrm{na}i}, S_{\mathrm{nb}i}, S_{\mathrm{nc}i} \end{bmatrix} \begin{bmatrix} 1 \\ 1 \\ 1 \end{bmatrix} = \begin{bmatrix} 1 \\ 1 \end{bmatrix} \tag{2}$$

in which i represents to the serial number of the module.

In each module, when the upper arm of a phase is ON, this phase correspondingly outputs a positive current level at the ac-side, while the lower bridge arm turning ON leads to a negative current level. Therefore, the algebraic sum of the three-phase current levels at ac-side of each module is zero

$$\sum_{\varphi=\mathrm{a}}^{c} N_{\mathrm{SM}i\varphi} = [1, -1] \begin{bmatrix} S_{\mathrm{pa}i}, S_{\mathrm{pb}i}, S_{\mathrm{pc}i} \\ S_{\mathrm{na}i}, S_{\mathrm{nb}i}, S_{\mathrm{nc}i} \end{bmatrix} \begin{bmatrix} 1 \\ 1 \\ 1 \end{bmatrix} = 0. \tag{3}$$

Then, for the whole MCSC, the algebraic sum of three-phases current levels at ac-side is also zero

$$\sum_{\varphi=\mathrm{a}}^{c} N_{\varphi} = \sum_{k=1}^{n} \sum_{\varphi=\mathrm{a}}^{c} N_{\mathrm{SM}k\varphi} = 0. \tag{4}$$

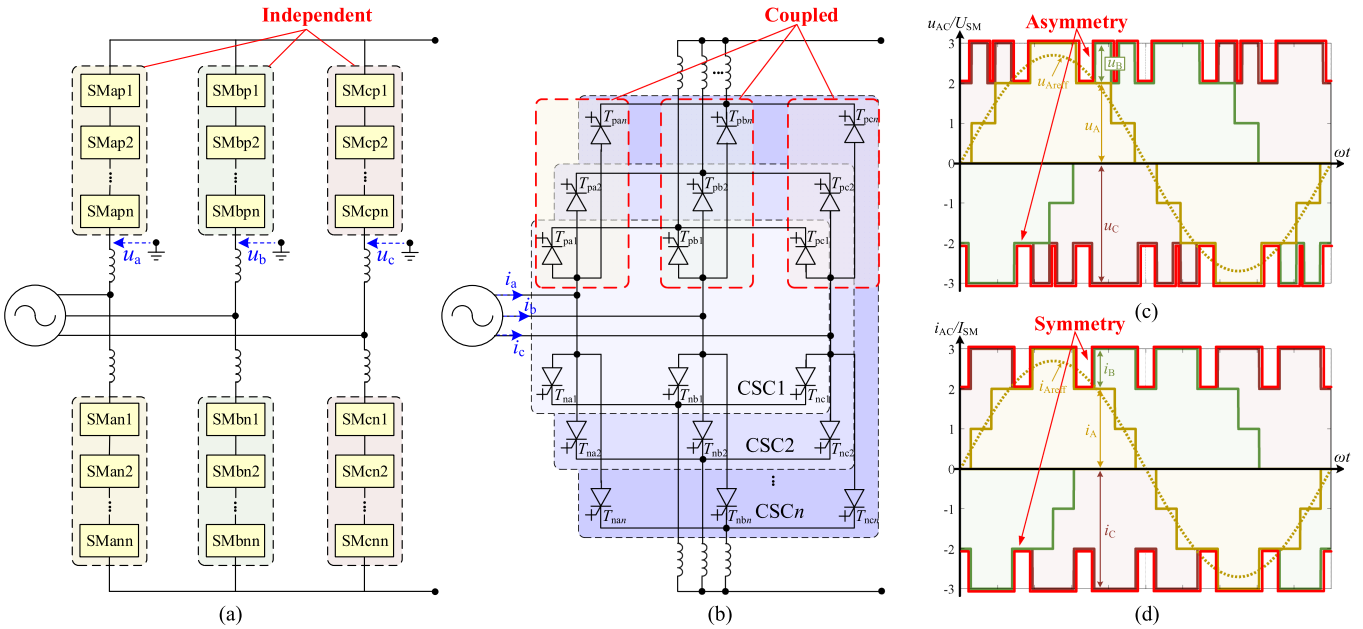

Fig. 1. Principle of proposed SCAM and comparation with NLM. (a) Topology of MMC with independent bridge arms. (b) Topology of MCSC with coupled bridge arms. (c) Schematic of NLM. Independent voltage modulation of different phases leads to asymmetry envelope (in red). (d) Schematic of SCAM. Topology constraint of sub-CSCs causes symmetry envelope.

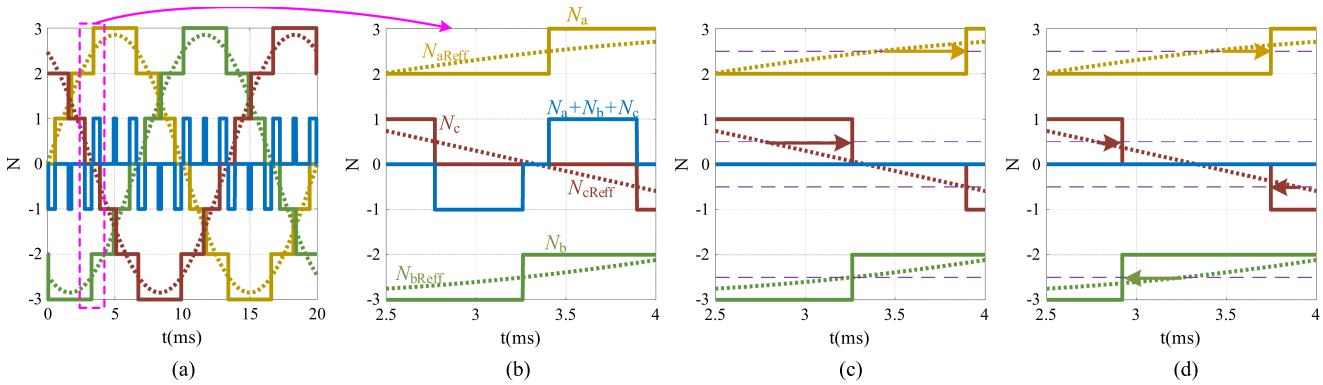

Fig. 2. (a) Discretized reference current (direct SCAM), which does not meet the constraint of MCSC topology. (b) Zoom in of (a). (c) Meeting MCSC topology constraint by delaying pulse (original SCAM). (d) Meeting MCSC topology constraint by modified SCAM based on reference current gradient (modified SCAM).

In three-phases-balanced state, the algebraic sum of the reference current keeps the constant of 0, which can theoretically meet the constraint. However, as SCAM rounds the reference current, the algebraic sum of three-phase current levels (N_a+N_b+N_c) will fluctuate ±1 because the rising and falling currents of different phases in a certain period do not exactly cross the threshold of k+1/2 at the same moment. It is against with the topology constraint, as is shown in Fig. 2(a) and (b).

A basic solution is to delay some of the switch behaviors. When the reference current of one phase crosses the threshold first, the current level does not change temporarily until the reference current of the other phase crosses the threshold inversely. Then, the current levels of the two phases step simultaneously, as shown in Fig. 2(c). This method is simple to implement, but will distort the current-level waveform. It increases harmonics, and adversely affects the control.

C. Modified SCAM Based on Reference Current Gradient

A modified SCAM based on reference current gradient is proposed to reduce the adverse effects of the previous scheme. When the reference current of one phase crosses the threshold, the other phase of which the current level will step inversely earliest is predicted by the gradient of the reference current. Then, the current levels of the two phases step together exactly when their reference currents deviate from the thresholds by the same value, as in Fig. 2(d).

In this scheme, long switching delay of one phase in the former scheme is replaced by short switching delay-and-advance of two phases, respectively. While meeting the topology constraint, the distortion of current waveform is reduced, and the harmonic degradation caused by meeting the topology constraints in the former scheme is decreased.

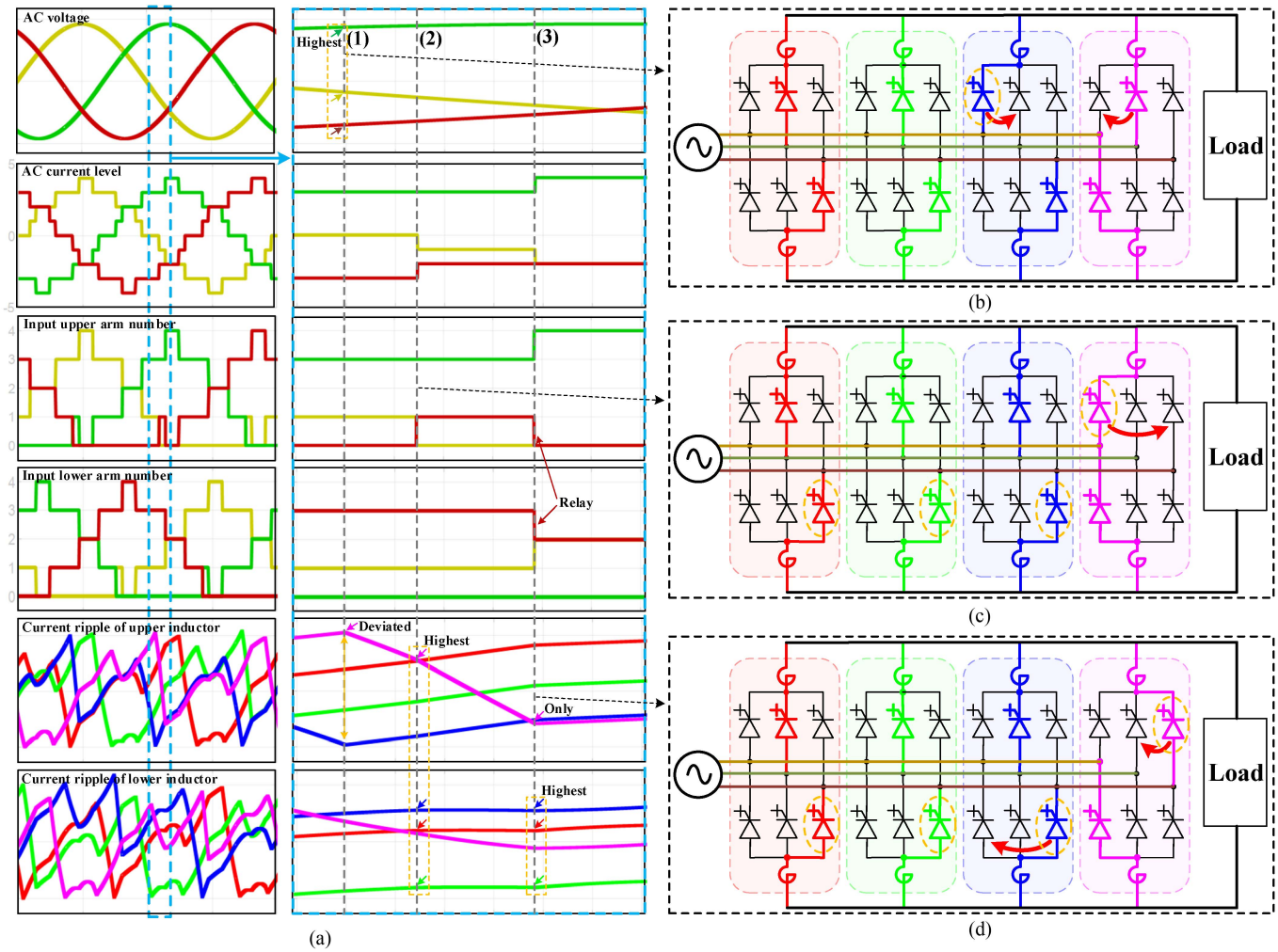

Fig. 3. Schematic of switching behavior in SCAM-based MCSC of four modules. (a) AC and DC waveforms and statistics of module state. (b) Additional exchange-switching for current balancing. (c) Switching behavior in AC current-level stepping. (d) Solution of switching dilemma.

III. Current Balancing Algorithm (CBA) of SCAM

A. CBA Principle in MCSC

Due to the switching sequence of modules, the volt-second product on dc inductors are not equal. Besides, deviation exists on different transistors and inductors. These factors lead to unbalanced current among modules. As a result, the harmonic of ac-side becomes worse, and the devices cannot be fully utilized. Therefore, active current balancing is necessary.

In MCSC, the positive and negative poles on the dc output port have relatively constant potentials separately, while the ac voltage of three phases constantly alternates. The current variation trend of the dc inductors can be adjusted by switching the bridge arms to connect the dc inductor to different phases of ac-side. In this way, the current of dc inductor in different modules can be controlled and restricted within a certain range to achieve current balancing.

For a positive dc inductor, being connected to a phase with higher instantaneous voltage will cause its current to rise, while being connected to a phase with lower instantaneous voltage will cause its current to fall. Conversely, for a negative dc inductor, higher instantaneous voltage means falling current while lower instantaneous voltage means rising current.

B. Switching Algorithm in AC Current-Level Stepping

In SCAM with CSC topology constraint, current levels of one phase rises and that of another phase falls meanwhile as they change. The current tendency of inductors after switching can be judged according to the polarity of the instantaneous line-voltage between the two phases. Then, the module having the highest dc current deviation in the upper or lower inductors and being able to be corrected by the switching is identified. The states of the arms at corresponding side of this module are switched.

As is shown in the stage (2) of Fig. 3(a), the current of phase-c rises by one level and the current of phase-a drops by one level. The operation can be either commutating one of the upper arms from phase-a to phase-c, or commutating one of the lower arms from phase-c to phase-a. Therefore, the modules with upper arm of phase-a conducting (only module 4) and the modules with lower arm of phase-c conducting (module 1, 2, and 3) are found.

Since $U_{ca}<0$, no matter the arms on which side are switched, the corresponding inductor current will fall. Hence, the currents of the inductors in the corresponding side of these modules are sorted and the highest one is found (upper inductor current of module 4). Finally, the upper arm of phase-a in module 4 is turned OFF and the upper arm of phase-c in this module is turned ON [see Fig. 3(c)].

C. Switching Dilemma and Solution

According to the algorithm in *part B*, when current level of phase-a steps down and that of phase-b steps up, either a module with upper bridge arm of phase-a conducting commutates to phase-b, or a module with lower bridge arm of phase-b conducting commutates to phase-a is acceptable. However, there is a case that neither of these modules exist. At this time, the required current level cannot be achieved by switching bridge arms on only one side of a module [see stage (3) in Fig. 3(a)].

As a solution, a module with upper bridge arm of phase-c conducting commutates to phase-b, meanwhile a module with lower bridge arm of phase-c conducting commutates to phase-a. In this way, the dilemma is solved by the "relay" of phase-c. If there are multiple modules with bridge arm of phase-c in either upper or lower side conducting, the operated modules can also be selected based on the order of instantaneous phase voltage and sort of inductor current to realize the correction of inductor current incidentally, as in Fig. 3(d).

The feasibility is demonstrated as follows: In the condition of nonovermodulation ($m < 1$), since the level of phase-a still decreases and there is no module with upper bridge arm of phase-a conducting at this time, it can be inferenced that not all the modules are with their lower arm of phase-a conducting (otherwise, the current level of phase-a is more than the total number of modules, which is against with nonovermodulation). On this basis, because there is no module with lower bridge arm of phase-b conducting either, at least one module with lower bridge arm of phase-c conducting exists. Similarly, it can also be deduced that at least one module with upper bridge arm of phase-c conducting exists. Therefore, the relay solution is always practicable.

D. Additional Exchange-Switching for Current Balancing

In the above strategy, the switching behaviors required by the modulation can be fully utilized to balance the inductor current as far as possible. However, due to the long period of ac cycle, it is not enough for current balancing to switch only when ac current-level steps, in which way a switched module may not be able to change its state in the coming half cycle and its current may be out of bounds.

Therefore, an additional current balancing strategy is set up. In each sampling period of the controller, the inductor currents at both sides of the modules are sorted separately. If the maximum or minimum current deviates from the average current of the modules over the set tolerance, the phase commutating to which can correct this deviation is found according to the instantaneous value of the ac voltage. Then, the module with the bridge arm of this phase at corresponding side conducting and has the highest inverse current deviation is selected. The switching state of the two modules is exchanged to realize current balancing [see Fig. 3(b)].

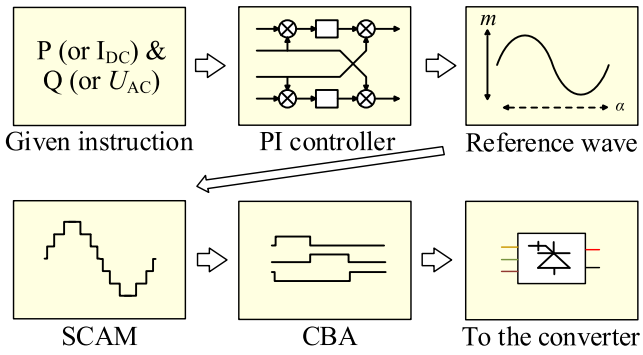

Fig. 4. Entire controller of MCSC based on SCAM.

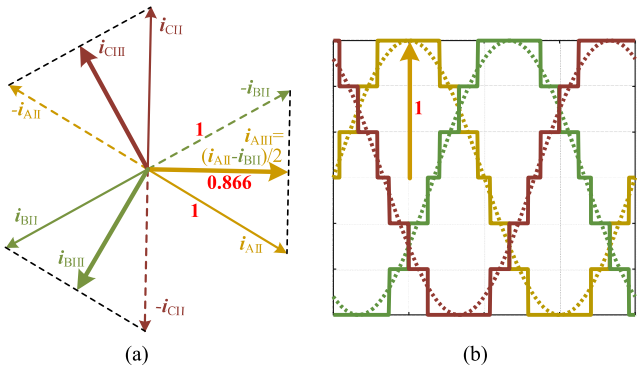

Fig. 5. DC current utilization factor. (a) SPWM. (b) SCAM.

The above strategy completely decouples the dc current control and ac modulation of the converter. It keeps the dc current of each module balanced with as little extra switching behavior as possible while the requirement of ac output current waveform is met. In addition, the current balance of both the upper and the lower inductors can be realized together, avoiding intermodule circulating current.

E. Entire Controller of MCSC Based on SCAM

The structure of MCSC controller is shown in Fig. 4. Given instruction is first processed in a classic *d-q* decoupling PI controller and transformed into modulation ratio (m) and phase-shifting angle (α). Then, reference current of the three phases is generated and then discretized into current levels by SCAM. Finally, pulse signal is distributed to modules according to CBA.

IV. Performance Analysis of SCAM

A. DC Current Utilization Factor

The dc current utilization factor is defined as the ratio of ac peak current to dc load current. In SPWM, a binary-triadic logic transformation is constructed to meet the topological constraints of current-source converters. It limits the maximum utilization factor to 0.866 [see Fig. 5(a)]. In the proposed SCAM, peak ac current can be achieved by the dc current superposition of all modules, as in Fig. 5(b). Therefore, the utilization factor can

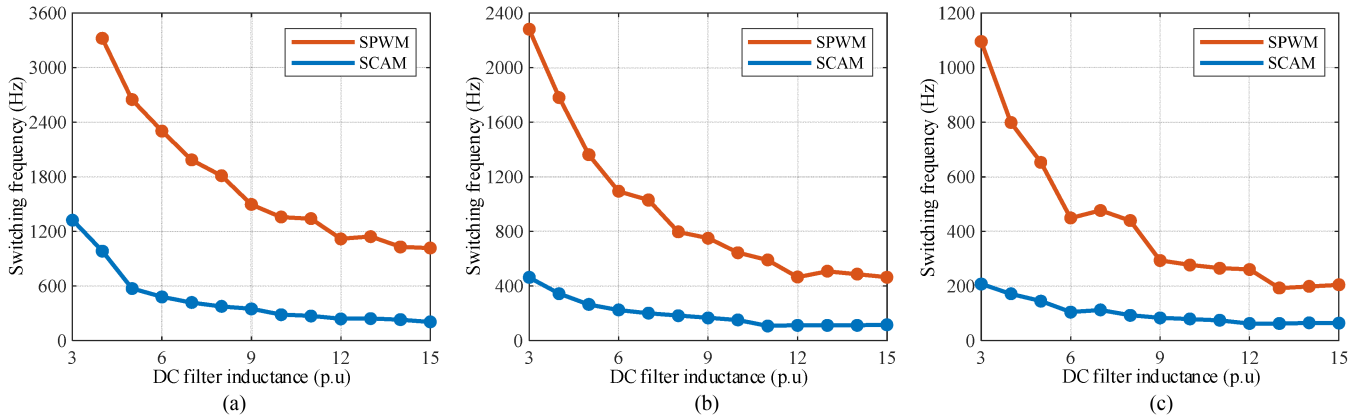

Fig. 6. Simulation results of switching frequency at fixed current imbalance ratio (r) based on SPWM and SCAM. (a) $r = \pm 5\%$. (b) $r = \pm 10\%$. (c) $r = \pm 20\%$.

TABLE I
SIMULATION PARAMETERS

Items	Value
Number of modules	8
Rated dc power	10 MW
Rated dc voltage	600 V
dc load	Pure resistive
Rated modulation ratio	0.95
AC voltage	515 V for SCAM (595 V for SPWM)
AC frequency	50 Hz
AC side equivalent inductance (grid and transformer)	0.355 pu
AC commutation capacitance	0.0834 pu

reach 1, which is 15.5% higher than that of SPWM and equal to schemes such as SVPWM.

Ignoring the loss, the power of ac input and dc output is equal in steady state, as

$$\sqrt{3}U_{\mathrm{ac}}I_{\mathrm{ac}}=U_{\mathrm{dc}}I_{\mathrm{dc}}. \tag{5}$$

For dc loads with the same voltage–current external characteristics, when SCAM is adopted, the ac voltage decreases by 13.4% compared with SPWM scheme, thus the blocking voltage of power electronic devices can be reduced.

B. DC Filter Inductance and Switching Frequency

Excessive differential current among modules leads to unbalanced thermal and electrical stress on transistors, resulting in the degradation of converter performance, such as capacity and efficiency. The algorithms have different ability for current balancing control. With the same current equalization standard, the strategy with poor control ability needs higher switching frequency and dc inductance.

The performance of proposed SCAM and level-switched-SPWM with the CBA of unified inductor-current sorting [31] is compared by simulation on Simulink. The parameters are shown in Table I.

The average switching frequency required to achieve the same current equalization standard under sequential dc inductances is obtained. The results at the current imbalance ratio of $\pm 5\%$, $\pm 10\%$, and $\pm 20\%$ are shown in Fig. 6(a)–(c) separately.

With the proposed SCAM, the switching frequency is reduced to less than 1/3 of the SPWM scheme in all cases. For imbalance ratio of $\pm 10\%$ and $\pm 20\%$, the switching frequency can reach the near-power frequency of around or even below 100 Hz. This feature is attributable to the step modulation waveforms in SCAM and the full use of each switching behavior for current balancing, which reduces unnecessary switching behavior as much as possible. In addition, in SCAM, current equalization standard is a variable that can be directly regulated while that of SPWM needs to be obtained through indirect calculation or analysis, for which SCAM suits engineering application better.

C. AC Harmonic

The current harmonics at the grid side under different module number and modulation ratio are simulated. The simulation parameters follow those in Table I except that the rated power varies linearly with the number of modules. In particular, the original SCAM is also simulated to verify the effect of the proposed reference-current-gradient-based SCAM. The current equalization standard of SCAM is set to $\pm 10\%$, and the carrier ratio (f/f_N) of SPWM is set to 15 and 35. The total demand distortion (TDD) with different modulation ratios (m) is shown in Fig. 7(a)–(c) separately.

The harmonic of SPWM-based MCSC is greatly affected by the modulation frequency, so high switching frequency is required to optimize the harmonic. The harmonic of SCAM-based MCSC is negatively correlated with the number of modules. When the number of modules is higher than 7, the TDD can meet the grid-connection requirement of 5% by IEEE standard [37]. Besides, the modified SCAM further optimizes the harmonic in some conditions.

V. EXPERIMENTAL VERIFICATION

A. Hardware-in-the-Loop Experiment Platform

A hardware-in-the-loop experiment platform is built to verify the feasibility and performance of the proposal, as shown in Fig. 8. The SCAM controller is implemented with an advanced RISC Machine (Xilinx-Zynq7015) to generate the modulation waveform and an FPGA (cycloneV-5CGXFC7) to realize CBA

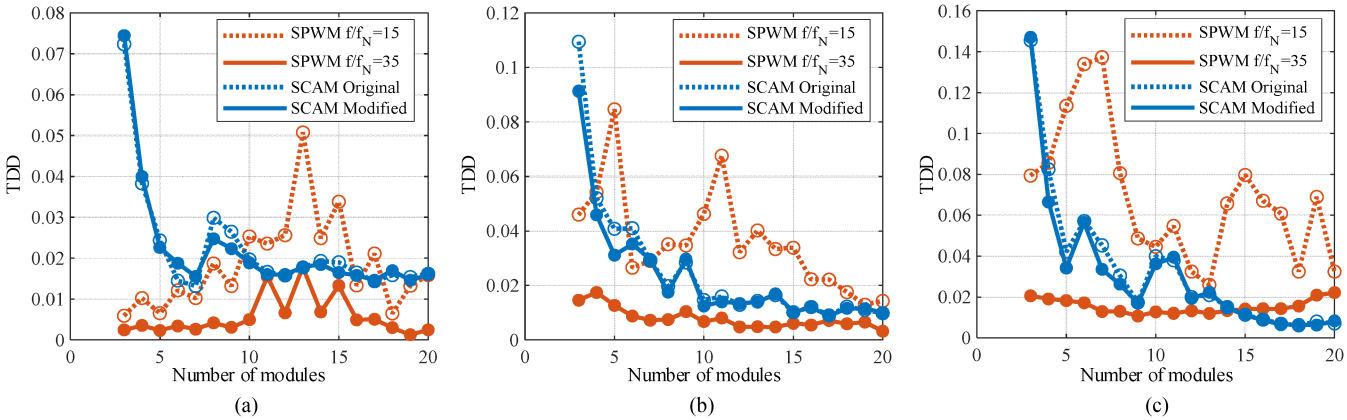

Fig. 7. TDD of two modulation methods at sequential module numbers. (a) $m = 0.2$ (slight load). (b) $m = 0.6$ (typical load). (c) $m = 0.95$ (rated full load).

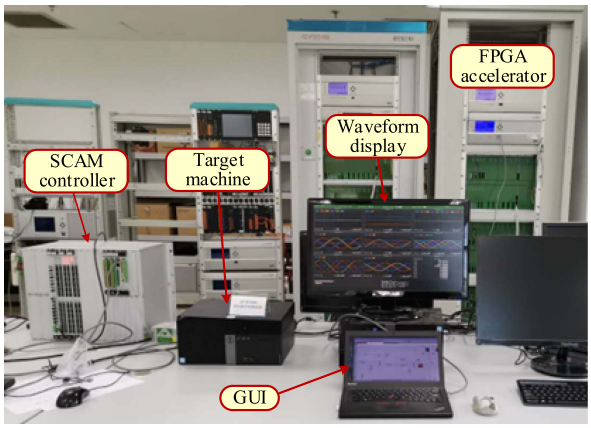

Fig. 8. Implemented SCAM controller and hardware-in-the-loop experiment platform.

and pulse allocation. In this platform, the primary circuit is built in GUI and emulated by FPGA to realize accelerated calculation with the fixed step size of 20 μs.

The parameters of the primary circuit are consistent with the simulation in Table I. The dc filter inductance is set as 7.1 pu (600 uH), and the current imbalance ratio is set to $\pm$150 A. In particular, a hydrogen–electrolyzer model is applied as the dc load, in which a voltage source representing both the reversible voltage and overpotential is series connected with a resistor to substitute the pure ohmic losses. The components are scaled up from the single electrolytic cell [9], [12], [38].

The SUNGROW SHR5700 power supply for electrolyzer reaches the rated output of 580 V and 7060 A [10], and the rated inputs of industrial electrolyzer SHME500A and SHME1000A are 364 V, 6600 A and 700 V, 6850 A separately [11]. Considering a parallel connection of two electrolyzers above or a growth potential of single electrolyzer in the future, the load parameter is also chosen as 600 V and 10 MW (16667 A), as shown in Table II.

B. Converter Mode Operation

The stable operation and dynamic process under different load rates are tested, and the waveform is shown in Fig. 9(a) and (b).

TABLE II
PARAMETERS OF ELECTROLYZER LOAD MODEL

Parameter	Single electrolytic cell	Electrolyzer model
Rated load	2.3V 4 A (per cm^2)	600 V 16667 A
Threshold voltage	1.5 V	391.3 V
Slope resistance	200 mΩ	12.52 mΩ

The SCAM-based MCSC has rapid response speed and can complete the power step within 0.1 s, for which it will be suitable for renewable-energy hydrogen-production scenario with highly fluctuating power. In particular, the zoomed waveforms at rated load are shown. The positive and negative dc current of the modules can achieve great balance within the set range. Benefit from the interleaving superposed output of each module, the load current ripple is within 2%. The grid-side ac current is highly sinusoidal. The switching frequency of the transistors in one submodule is detected, which fluctuates within a certain range, and the average frequency is about 65 Hz.

C. Reactive Compensation Ability and STATCOM Operation

The reactive power control ability of SCAM is further verified. In Fig. 9(c), the MCSC operates under full active-power load, unit power factor (UPF), and reactive compensation for grid using redundant modulation ratio successively before 1.5 s. Then, between 1.5 and 2 s, the converter is blocked and the dc load is bypassed, transforming the MCSC converter to an MCSC-STATCOM. After 2 s, the device operates in STATCOM mode with different reactive power. It is worth noting that MCSC-STATCOM operates at rated modulation ratio and low dc current under slight load rather than full dc current, thus reducing the power loss and optimizing ac harmonic.

VI. DISCUSSION

A. Efficiency of SCAM-Based MCSC

The power-electronic-part power loss of the above 10-MW SCAM-based MCSC is theoretically analyzed. The voltage and current of the switching behavior of power-electronic devices are extracted and converted linearly according to the nominal value in the datasheet of the devices to obtain the switching loss.

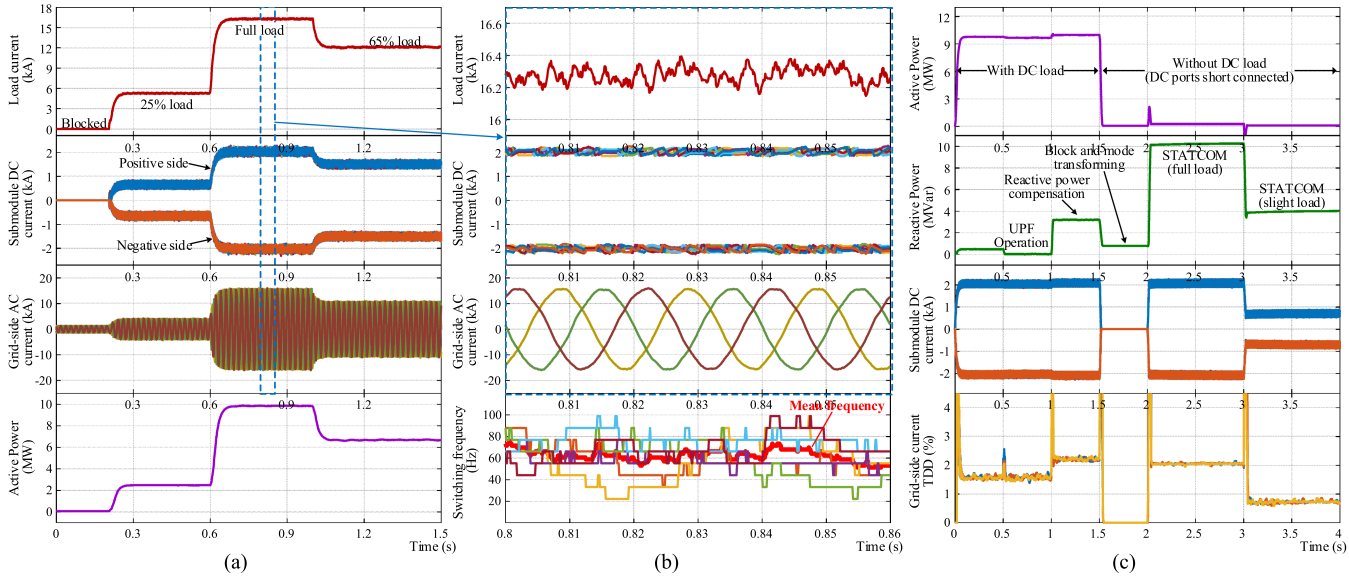

Fig. 9. Hardware-in-the-loop experimental waveforms on SCAM-based MCSC. (a) Stable operation and dynamic process at converter mode. (b) Zoom-in waveform. (c) Reactive-power control and STATCOM operation.

TABLE III
PARAMETERS OF THE APPLIED DEVICES IN LOSS ANALYSIS

Device	IGBT	Diode	IGCT
Threshold voltage/V	0.748	1.210	0.781
Slope resistance/mΩ	0.260	0.188	0.146
Turn-on energy/J	0.205	\	1
Turn-off energy/J	0.845	\	50
Reverse recovery energy/J	\	0.150	22.5
Nominal voltage/V	600	600	1700
Nominal current/A	2400	2400	3000

ON-state loss is calculated by actual current, nominal threshold voltage, and slope resistance of the device [39].

Both IGBT and IGCT schemes are adopted in the evaluation. The IGBT with diode is Infineon FF2400RB12IP7P [40], and the IGCT is ABB 5SHZ-60L2500 [41], both of which are the latest available devices. Because the IGCT is reverse-blocking type, it does not need a diode in series in MCSC application [42]. There main parameters are shown in Table III.

Then, the power loss is compared with that of not only the traditional SPWM–MCSC, but also the PWM–VSC, in which an additional buck circuit is considered to realize a continuous adjustable output. Since the auxiliary components are all used in these schemes, such as the inductors and the grid-link transformers, these factors are ignored. The mean switching frequency of SCAM-based MCSC is 100 Hz, while that of SPWM–MCSC is 750 Hz. The modulation frequencies of PWM–VSC and the attached buck circuit are both 1000 Hz [10], [18].

Detailed results are shown in Fig. 10, in which the total loss rates are also marked on the bars separately. Although the loss-rate of IGBT-based PWM–VSC is relatively low, it is increased by the attached buck circuit, which is then a little worse than that of IGBT-based SPWM–MCSC. With the proposed SCAM, the reduction of switching loss provides an efficiency advantage. This efficiency advantage is further amplified by the IGCT and reaches to 0.70%, which is better than any other schemes,

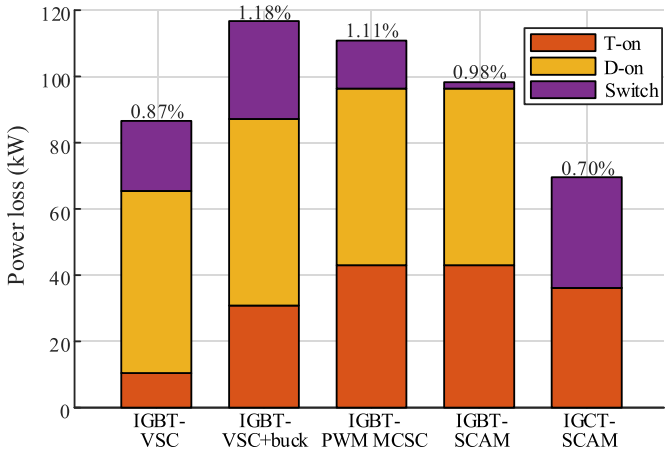

Fig. 10. Power loss analysis of electrolyzer-power-supply schemes.

benefiting from the bidirectional conductance modulation effect and reverse-bocking ability of IGCT. Since the IGCT applied still has a certain voltage margin, the output voltage can be increased to 1000 V, and the efficiency will be more optimized to 0.55%.

B. Harmonic Influence Mechanism of Modified SCAM

According to Fig. 7, the modified SCAM is effective in reducing TDD under some conditions. The harmonic spectrum of eight module MCSC at converter port and grid port based on original and modified SCAM is further analyzed, as shown in Fig. 11. The modified method reduces the long step-jump delay caused by the topological constraints of CSC in some cases through derivative prediction and optimizes the symmetry of modulation waveform. Therefore, the low-order harmonics is effectively reduced, especially the 5, 7, and 11 order and even-order harmonics. Since the commutation capacitors and

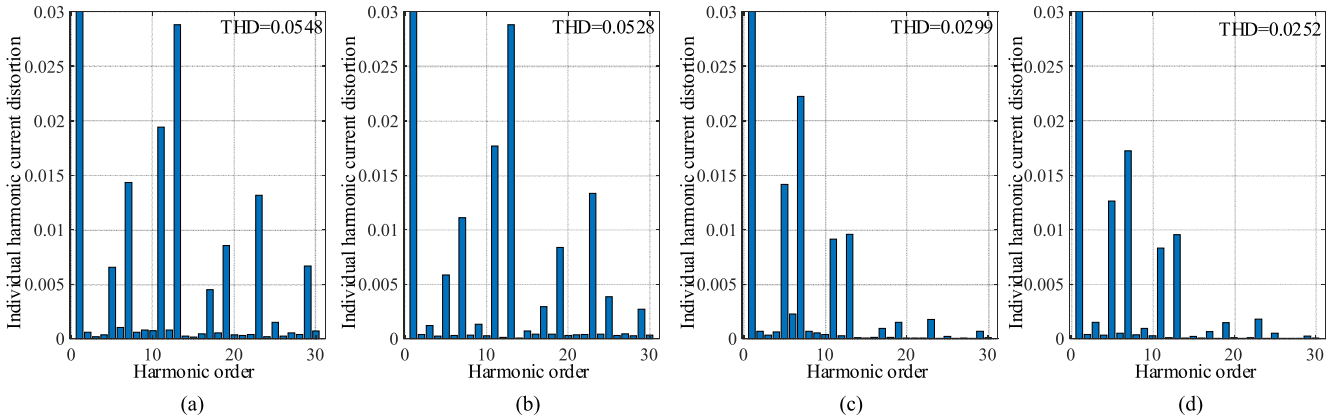

Fig. 11. Harmonic spectrum of eight module MCSC. (a) Original SCAM and converter port. (b) Modified SCAM and converter port. (c) Original SCAM and grid port. (d) Modified SCAM and grid port.

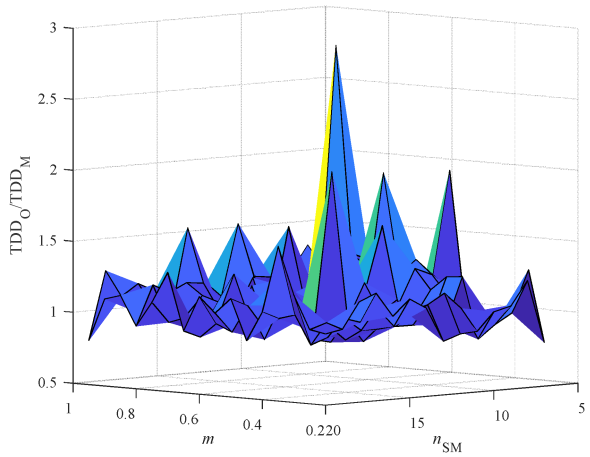

Fig. 12. Ratio of TDD with original SCAM to that of modified SCAM.

the equivalent inductors of ac source constitute a low-pass filter, the high-order harmonics are easier filtered. As a result, modified SCAM leads to lower grid-side harmonic

However, in a few conditions, one or more of the low-order harmonic contents, especially 5th, 7th, and 11th may coincidently be low due to the specific combination of modulation ratio and module number. In these individual cases, the proposed method cannot improve TDD, but even increase TDD slightly due to the destruction of such coincidence.

To further prove the argument above, the grid-side TDD of SCAM-based MCSC before and after modification with different module numbers (n_{SM}) suitable for SCAM ($\geq$7) and denser modulation ratios (m) is analyzed in Simulink. The results are shown in Fig. 12, which intuitively demonstrates that the positive effect of the modification on TDD is greater than the negative effect. Further statistics indicate that 82 of the 224 data had TDD optimized by more than 10%, while only 13 had TDD aggravated by more than 10%. Furthermore, 30 optimized by more than 20%, and none aggravated by more than 20%. The mean TDD before and after modification is 1.75% and 1.61%, respectively. It proves the effectiveness of the modification in optimizing harmonic characteristics.

VII. Conclusion

MCSC has potential prospects in high-current variable-voltage application. The proposed SCAM can maintain dc current balance between modules with power electronic devices switching at near-power-frequency. It brings an opportunity for the use of reverse-blocking devices with lower ON-state voltage. When the number of modules is higher than 7, the grid-side TDD can meet the requirement of 5%, without the need of high switching frequency. The feasibility of SCAM-based MCSC is verified on hardware-in-the-loop experiment platform with a typical 10-MW hydrogen–electrolyzer load. It realizes steady operation and rapid power step, as well as UPF operation and reactive compensation. The efficiency of SCAM-based MCSC is expected to improve significantly.

The further article can focus on the hardware level to take full advantage of SCAM, for example, the design, implementation, and experiment of MCSC based on reverse-blocking devices.

References

[1] V. Fediakov, G. Gavritukhin, and I. Golovan', "Comparison of thyristor and transistor topologies of converters for electrolysis on the example of a cadmium electrolysis system," in *Proc. IEEE Int. Ural Conf. Elect. Power Eng.*, 2021, pp. 577–581.

[2] E. P. Wiechmann, P. E. Aqueveque, L. G. Muñoz, J. A. Henríquez, and A. S. Morales, "Technical assessment of industrial operation of copper electrowinning cells with current source topology," in *Proc. IEEE Ind. Appl. Soc. Annu. Meeting*, 2013, pp. 1–5.

[3] I. R. Abdulveleev, G. P. Kornilov, and T. R. Khramshin, "Research of DC electric arc furnace with commutated power circuit," in *Proc. IEEE Int. Conf. Ind. Eng., Appl. Manuf.*, 2020, pp. 1–7.

[4] M. Lehner et al., "The power-to-gas concept," in *Power-to-Gas: Technology and Business Models*. Berlin, Germany: Springer-Verlag, 2014, pp. 7–17.

[5] F. Dawood, M. Anda, and G. M. Shafiullah, "Hydrogen production for energy: An overview," *Int. J. Hydrogen Energy*, vol. 45, no. 7, pp. 3847–3869, Feb. 2020.

[6] C. Baumann, R. Schuster, and A. Moser, "Economic potential of power-to-gas energy storages," in *Proc. IEEE 10th Int. Conf. Eur. Energy Market*, 2013, pp. 1–6.

[7] H. Renaudineau, A. M. Llor, R. Cortés D., C. A. Rojas, C. Restrepo, and S. Kouro, "Photovoltaic green hydrogen challenges and opportunities: A power electronics perspective," *IEEE Ind. Electron. Mag.*, vol. 16, no. 1, pp. 31–41, Mar. 2022.

[8] J. Solanki et al., "High-current variable-voltage rectifiers: State of the art topologies," *Inst. Eng. Technol. Power Electron.*, vol. 8, no. 6, pp. 1068–1080, 2015.
[9] M. Keddar et al., "Power quality improvement for 20 MW PEM water electrolysis system," *Int. J. Hydrogen Energy*, vol. 47, no. 95, pp. 40184–40195, Dec. 2022.
[10] "IGBT-based rectifier for electrolyzer power supply," 2022. [Online]. Available: https://www.sungrowpower.com/hydrogenproduction/product/28/152.html
[11] "Alkaline electrolyzer for hydrogen production," 2023. [Online]. Available: https://www.sungrowpower.com/hydrogenproduction/product/29/68.html
[12] F. W. Speckmann, S. Bintz, and K. P. Birke, "Influence of rectifiers on the energy demand and gas quality of alkaline electrolysis systems in dynamic operation," *Appl. Energy*, vol. 47, pp. 855–863, Sep. 2019.
[13] J. Koponen, V. Ruuskanen, A. Kosonen, M. Niemelä, and J. Aho, "Effect of converter topology on the specific energy consumption of alkaline water electrolyzers," *IEEE Trans. Power Electron.*, vol. 34, no. 7, pp. 6171–6182, Jul. 2019.
[14] P. Ladoux, G. Postiglione, H. Foch, and J. Nuns, "A comparative study of AC/DC converters for high-power DC arc furnace," *IEEE Trans. Ind. Electron.*, vol. 52, no. 3, pp. 747–757, Jun. 2005.
[15] S. Yang, J. Wang, and W. Yang, "A novel 24-pulse diode rectifier with an auxiliary single-phase full-wave rectifier at DC side," *IEEE Trans. Power Electron.*, vol. 32, no. 3, pp. 1885–1893, Mar. 2017.
[16] V. Ruuskanen et al., "Power quality and reactive power of water electrolyzers supplied with thyristor converters," *J. Power Sources*, vol. 459, May 2020, Art. no. 228075.
[17] L. Monroy-Morales et al., "Modeling and control design of a Vienna rectifier based electrolyzer," in *Proc. IEEE 7th Int. Symp. Power Electron. Distrib. Gener. Syst.*, 2016, pp. 1–8.
[18] J. Koponen et al., "Comparison of thyristor and insulated-gate bipolar transistor-based power supply topologies in industrial water electrolysis applications," *J. Power Sources*, vol. 491, Apr. 2021, Art. no. 229443.
[19] X. Guo et al., "A new multi-mode fault-tolerant operation control strategy of multiphase stacked interleaved Buck converter for green hydrogen production," *Int. J. Hydrogen Energy*, vol. 47, no. 71, pp. 30359–30370, Aug. 2022.
[20] S. Bintz et al., "Parallel-serial-rectifier for power-to-hydrogen applications," in *Proc. 21st Eur. Conf. Power Electron. Appl.*, 2019, pp. P.1–P.11.
[21] X. Meng, M. Chen, M. He, X. Wang, and J. Li, "A novel high power hybrid rectifier with low cost and high grid current quality for improved efficiency of electrolytic hydrogen production," *IEEE Trans. Power Electron.*, vol. 37, no. 4, pp. 3763–3768, Apr. 2022.
[22] K. Gnanasambandam, A. K. Rathore, A. Edpuganti, D. Srinivasan, and J. Rodriguez, "Current-fed multilevel converters: An overview of circuit topologies, modulation techniques, and applications," *IEEE Trans. Power Electron.*, vol. 32, no. 5, pp. 3382–3401, May 2017.
[23] Z. Bai and Z. Zhang, "Conformation of multilevel current source converter topologies using the duality principle," *IEEE Trans. Power Electron.*, vol. 23, no. 5, pp. 2260–2267, Sep. 2008.
[24] M. P. Aguirre, L. Calvino, and M. I. Valla, "Multilevel current-source inverter with FPGA control," *IEEE Trans. Ind. Electron.*, vol. 60, no. 1, pp. 3–10, Jan. 2013.
[25] J. Bao, W. Bao, Z. Zhang, and W. Fang, "A simple current-balancing method for a three-phase 5-level current-source inverter," in *Proc. IEEE 35th Annu. Conf. Ind. Electron.*, 2009, pp. 104–108.
[26] M. C. Chandorkar, D. M. Divan, and R. H. Lasseter, "Control techniques for multiple current source GTO converters," *IEEE Trans. Ind. Appl.*, vol. 31, no. 1, pp. 134–140, Jan./Feb. 1995.
[27] Z. Bai, Z. Zhang, and Y. Zhang, "A generalized three-phase multilevel current source inverter with carrier phase-shifted SPWM," in *Proc. IEEE Power Electron. Specialists Conf.*, 2007, pp. 2055–2060.
[28] L. Ding and Y. W. Li, "Simultaneous DC current balance and CMV reduction for parallel CSC system with interleaved carrier-based SPWM," *IEEE Trans. Ind. Electron.*, vol. 67, no. 10, pp. 8495–8505, Oct. 2020.
[29] M. M. Bhesaniya, A. Shukla, and G. D. Demetriades, "A control method for inductor current balancing in current source modular multilevel converter," in *Proc. IEEE IECON 41st Annu. Conf. Ind. Electron. Soc.*, 2015, pp. 002926–002931.
[30] M. M. Bhesaniya and A. Shukla, "Current source modular multilevel converter: Detailed analysis and STATCOM application," *IEEE Trans. Power Del.*, vol. 31, no. 1, pp. 323–333, Feb. 2016.
[31] F. Alskran and M. G. Simões, "Multilevel current source converter-based STATCOM suitable for medium-voltage applications," *IEEE Trans. Power Del.*, vol. 36, no. 2, pp. 1222–1232, Apr. 2021.
[32] C. Xu et al., "Comprehensive analysis and experiments of RB-IGCT, IGCT with fast recovery diode and standard recovery diode in hybrid line-commutated converter for commutation failure mitigation," *IEEE Trans. Ind. Electron.*, vol. 70, no. 2, pp. 1126–1139, Feb. 2023.
[33] L. Ding, Z. Quan, and Y. W. Li, "General Bi-Tri logic SPWM for current source converter with optimized zero-state replacement," *IEEE Trans. Power Electron.*, vol. 36, no. 10, pp. 11372–11382, Oct. 2021.
[34] L. Ding and Y. W. Li, "Multilevel CSC system based on series-parallel connected three-phase modules with optimized carrier-shift SPWM," *IEEE Trans. Power Electron.*, vol. 36, no. 4, pp. 3957–3966, Apr. 2021.
[35] L. M. Tolbert, F. Z. Peng, and T. G. Habetler, "Multilevel converters for large electric drives," *IEEE Trans. Ind. Appl.*, vol. 35, no. 1, pp. 36–44, Jan./Feb. 1999.
[36] S. Rohner, S. Bernet, M. Hiller, and R. Sommer, "Modulation, losses, and semiconductor requirements of modular multilevel converters," *IEEE Trans. Ind. Electron.*, vol. 57, no. 8, pp. 2633–2642, Aug. 2010.
[37] "*IEEE Recommended Practice and Requirements for Harmonic Control in Electric Power Systems*," IEEE Std 519-2014 (Revision of IEEE Std 519-1992), pp. 1–29, Jun. 2014.
[38] D. F. R. Diaz, E. Valenzuela, and Y. Wang, "A component-level model of polymer electrolyte membrane electrolysis cells for hydrogen production," *Appl. Energy*, vol. 321, Sep. 2022, Art. no. 119398.
[39] B. Zhao et al., "Practical analytical model and comprehensive comparison of power loss performance for various MMCs based on IGCT in HVDC application," *IEEE J. Emerg. Sel. Topics Power Electron.*, vol. 7, no. 2, pp. 1071–1083, Jun. 2019.
[40] "FF2400RB12IP7P," 2022. [Online]. Available: https://www.infineon.com/cms/en/product/power/igbt/igbt-modules/ff2400rb12ip7p/
[41] "Data sheet 5SYA 1260-03 Dec. 22: 5SHZ 60L2500," 2023. [Online]. Available: https://www.hitachienergy.com/us/en/products-and-solutions/semiconductors/integrated-gate-commutated-thyristors-igct
[42] R. Bai et al., "PWM-current source converter based on IGCT-in-series for DC Buck and constant-current application: Topology, design, and experiment," *IEEE Trans. Ind. Electron.*, vol. 70, no. 5, pp. 4865–4874, May 2023.

Ruihang Bai (Graduate Student Member, IEEE) was born in Xi'an, China, in 1998. He received the B.S. degree in electrical engineering, in 2020, from the Tsinghua University, Beijing, China, where he is currently working toward the Ph.D. degree in electrical engineering.

His research interests include high power converter, high power semiconductor device, and VSC–HVdc system.

Biao Zhao (Senior Member, IEEE) was born in Hubei, China, in 1987. He received the B.S. degree from the Dalian University of Technology, Dalian, China, in 2009, and the Ph.D. degree from the Tsinghua University, Beijing, China, in 2014, both in electrical engineering.

He is currently an Associate Professor with the Department of Electrical Engineering, Tsinghua University, Beijing, China. His research interests include high power converter, high power semiconductor device, and flexible dc transmission and distribution system.

Tianji Zhou was born in Wuhan, China, in 2001. He received the B.S. degree in electrical engineering, in 2022, from the Tsinghua University, Beijing, China, where he is currently working toward the Ph.D. degree in electrical engineering.

His research interests include high-power converters, renewable energy systems, and flexible dc transmission systems.

Jikang Wang was born in Liaoning, China, in 1995. He received the B.S. degree from the North China Electric Power University, Beijing, China, in 2016, and the M.S. degree from the Tsinghua University, Beijing, China, in 2019, both in electrical engineering.

He is currently working with the Beijing Sifang Automation Company, Ltd., Beijing, China. His research interests include dc distribution network, renewable energy, and medium-voltage power conversion system.

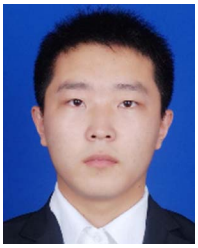

Yiqing Ma (Graduate Student Member, IEEE) was born in Shanxi, China, in 1999. He received the B.S. degree in electrical engineering from the Huazhong University of Science and Technology, Wuhan, China, in 2021. He is currently working toward the Ph.D. degree in electrical engineering with the Tsinghua University, Beijing, China.

His research interests include solid-state transformers, high power semiconductor device, and soft switching.

Guangke Lin was born in Shaanxi, China, in 1987. He received the B.S. degree in mechanical engineering from the Chendu University of Technology, Sichuan, China, in 2010, and the M.S. degree in electrical engineering from the Huazhong University of Science and Technology, Hubei, China, in 2012.

He is currently an Engineer with the Huairou Laboratory, Beijing, China. His research interest includes power-electronic converter equipment.

Yi Wang was born in Heilongjiang, China, in 1987. He received the B.S. and Ph.D. degrees in electrical engineering from the Tsinghua University, Beijing, China, in 2010 and 2016, respectively.

He is currently working with the Beijing Sifang Automation Company, Ltd., Beijing, China. His research interests include power electronic converter equipment and control systems for ac/dc hybrid distribution network.

Zhanqing Yu (Member, IEEE) was born in Inner Mongolia, China, in 1981. He received the B.Sc. and Ph.D. degrees in electrical engineering from the Tsinghua University, Beijing, China, in July 2003 and July 2008, respectively.

In July 2008, he became a Postdoctor with the Department of Electrical Engineering, Tsinghua University, Beijing, China, where he became a Lecturer in 2010 and an Associate Professor in 2012. His research interests include dc grid, dc breaker, electromagnetic environment and electromagnetic compatibility, and lightning protection.

Rong Zeng (Senior Member, IEEE) was born in Shaanxi, China, in 1971. He received the B.Eng., M.Eng., and Ph.D. degrees from the Department of Electrical Engineering, Tsinghua University, Beijing, China, in 1995, 1997, and 1999, respectively, all in electrical engineering.

In 1999, he was a Lecturer with the Department of Electrical Engineering, Tsinghua University, where he became an Associate Professor in 2002 and a Professor in 2007. He is currently working in the fields of airgap discharge, lightning protection, and electromagnetic compatibility in power systems, electric and magnetic field measurement by integrated electro-optical sensors, power semiconductor, HVdc system, and direct current circuit breaker.